Tectonophysics 671 (2016) 63–75

Contents lists available at ScienceDirect

Tectonophysics

journal homepage: www.elsevier.com/locate/tecto

Rock uplift at the transition from flat-slab to normal subduction: The Kenai Mountains, Southeast Alaska

Joshua D. Valentino [a,*], James A. Spotila [a], Lewis A. Owen [b], Jamie T. Buscher [c,d]

[a] Department of Geosciences, 4044 Derring Hall, Virginia Tech, Blacksburg, VA 24061, USA
[b] Department of Geology, University of Cincinnati, Cincinnati, OH 45221, USA
[c] Andean Geothermal Center of Excellence (CEGA), Universidad de Chile, Plaza Ercilla 803, Santiago, Chile
[d] Department of Geology, Facultad de Ciencias Físicas y Matemáticas, Universidad de Chile, Plaza Ercilla 803, Santiago, Chile

ARTICLE INFO

Article history:
Received 15 August 2015
Received in revised form 8 January 2016
Accepted 11 January 2016
Available online 29 January 2016

Keywords:
Flat slab subduction
Kenai Peninsula
Low-temperature thermochronometry
Exhumation
Topography

ABSTRACT

The process of flat-slab subduction results in complex deformation of overlying forearcs, yet how this deformation decays with distance away from the zone of underthrusting is not well understood. In south central Alaska, flat-slab subduction of the Yakutat microplate drives shortening and rock uplift in a broad coastal orogenic belt. Defined limits of the zone of underthrusting allow testing how orogenesis responds to the transition from flat-slab to normal subduction. To better understand forearc deformation across this transition, apatite (U–Th)/He low temperature thermochronometry is used to quantify the exhumation history of the Kenai Mountains that are within this transition zone. Measured ages in the northern Kenai Mountains vary from 10–20 Ma and merge with the exhumation pattern in the Chugach Mountains to the northeast, where high exhumation occurs due to flat-slab-related deformation. In the southern Kenai Mountains, however, ages increase to 30–50 Ma across a transition near Seward, Alaska, above the zone from flat-slab to normal subduction. These ages are relatively old in comparison to ages determined in other studies in southern Alaska and suggest minimal exhumation. Furthermore, transitions in topographic expression of the coastal orogen also occur at the margin of Yakutat underthrusting. These observations suggest that either deformation associated with flat-slab subduction requires tens of kilometers to decay with distance away from the zone of underthrusting, or that orogenesis in the Kenai Mountains is driven by a distinct tectonic cause. A potential driver of deformation is underplating of thick sediments, specifically the Surveyor Submarine Fan, along the Aleutian Megathrust, analogous to the tectonic mechanism responsible for the emergence of the Kodiak Island forearc. If correct, this may represent a recent tectonic transition in the region, given the minimal exhumation of the rugged Kenai Mountains despite the presence of an erosion-conducive glacial climate.

1. Introduction

Deformation in the upper plate of subduction zones relates to the orientation and morphology of the down-going plate (Fisher et al., 1998; Brandon et al., 1998; Dominguez et al., 2000). Lateral transitions in slab dip and morphology along a trench can lead to complex patterns of forearc development and uplift. For example, a change in subduction angle from steep to flat-slab may cause a gradual increase in upper plate shortening and rock uplift (Gutscher et al., 2000). Instances of flat-slab subduction in Central America and the Andes show that widespread deformation and uplift above the flat section decreases in intensity with gradual increase in subduction angle (Gutscher et al., 2000; Ramos et al., 2002). How upper plates respond along sharp transitions in slab subduction and geometry is less well known.

The Kenai Peninsula is part of a ~2000 km long exhumed accretionary prism and forearc along the southern margin of Alaska (Fig. 1) (Plafker et al., 1989). The region undergoes active rock uplift related to flat slab subduction, oblique collision, and accretion of the Yakutat microplate (Plafker and Berg, 1994; Haeussler et al., 2000). Intense deformation and exhumation occurs in the Wrangellia–St. Elias and Chugach Mountains, which are undergoing accretion directly related to Yakutat collision (Spotila and Berger, 2010; Arkle et al., 2013; Enkelmann et al., 2015). The mountainous forearc continues beyond the Yakutat microplate to where normal subduction of the Pacific plate occurs along the Aleutian Megathrust. The coastal mountains are rugged, have high topography (mean elevation 1000 m above sea level [asl]), and are deeply incised by glaciers (Buscher et al., 2008). The Kenai Mountains span both the western limit of the Yakutat plate and normal Pacific plate subduction, providing a unique opportunity to study

* Corresponding author.
E-mail addresses: joshua1@vt.edu (J.D. Valentino), spotila@vt.edu (J.A. Spotila), owenls@ucmail.uc.edu (L.A. Owen), jbuscher@vt.edu (J.T. Buscher).

http://dx.doi.org/10.1016/j.tecto.2016.01.022
0040-1951/

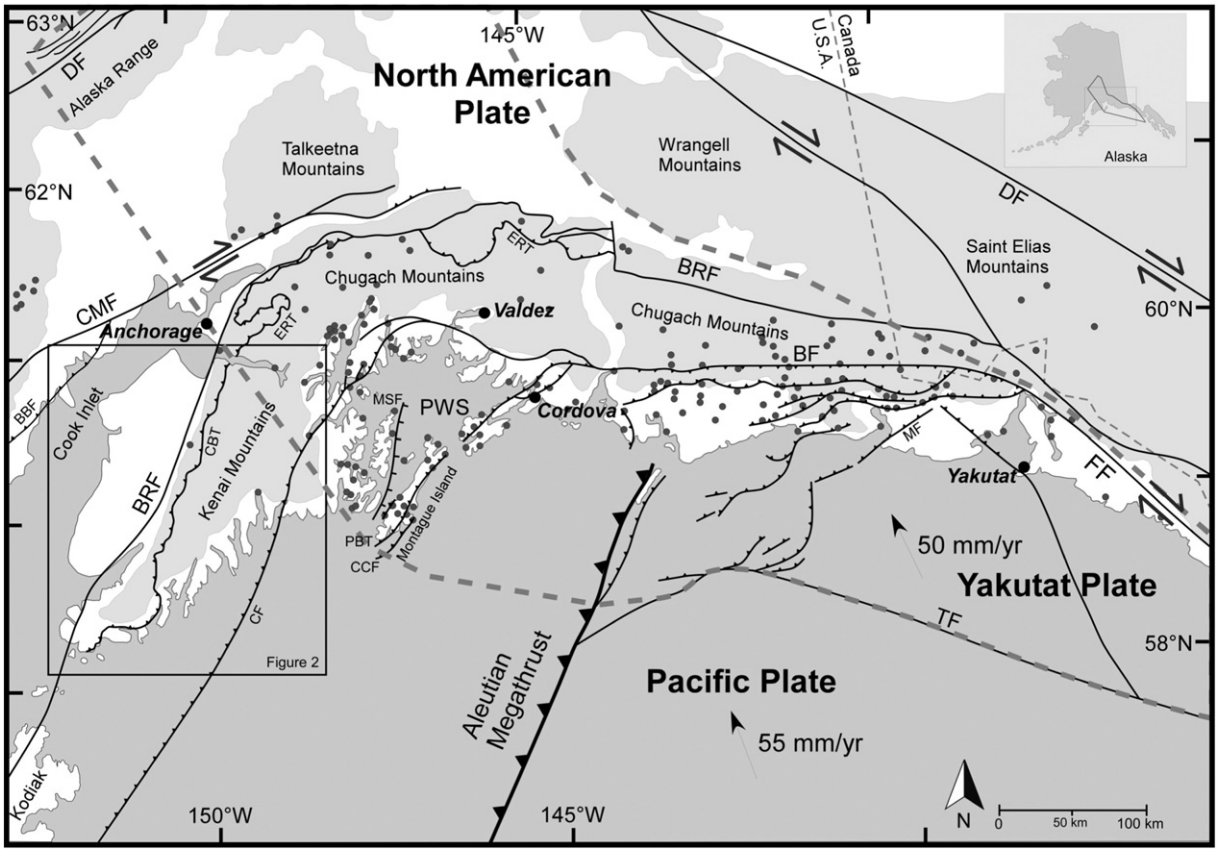

Fig. 1. Generalized tectonic map of major orogens, faults and plate boundaries, and localities mentioned in text throughout south central Alaska. The gray dots depict the distribution of AHe ages from previous studies. Plate motion vectors are from Elliott et al. (2010) for Yakutat Plate and Plattner et al. (2007) for the Pacific Plate. The thick gray dashed line shows the limit of the underthrust Yakutat microplate (Eberhart-Phillips et al., 2006; Fuis et al., 2008). Fault line thicknesses indicate major (thick) to relatively more minor (thinner) activity. BF = Bagley Fault, BRF = Border Ranges Fault, CCF = Cape Cleare Fault, CMF = Castle Mountain Fault, CBT = Chugach Bay Thrust, CF = Contact Fault, DF = Denali Fault, ERT = Eagle River Thrust, FF = Fairweather Fault, MSF = Montague Strait Fault, PBT = Patton Bay Thrust, PWS = Prince William Sound.

deformation across a sharp transition in down going slab geometry and morphology.

The approach of this study is to provide a first order constraint on the timing and magnitude of exhumation across the Kenai Mountains from which no previous thermochronometry has been documented. We measured apatite (U–Th)/He ages (AHe) across the Kenai Peninsula to test the effect of the slab transition on deformation of the forearc. Specifically, we sought to test whether a localized zone of rapid rock uplift occurred outside of the lateral transition zone away from the Yakutat plate, as suggested by the distribution of rugged topography. Our results using difficult lithologies provide the first quantitative values for exhumation associated with the unique tectonic transition.

2. Background

2.1. Flat slab subduction in Southern Alaska

Flat slab subduction drives upper plate deformation and orogenesis that can penetrate hundreds of kilometers into overriding continental lithosphere (English et al., 2003; Li and Li, 2007; Ramos et al., 2002). The common view is that flat slab subduction is linked to buoyant oceanic crust associated with thickened oceanic plateaus, hot-spot trails, or rapidly subducting, young slabs. After onset of flat slab subduction, upper plate shortening propagates landward and drives exhumation and broad surface uplift of the forearc, magmatic arc, and back arc basin, development of fold-thrust belts with widespread fault reactivation, and migration of arc volcanism (Little and Naeser, 1989; Berger et al., 2008; Gutscher et al., 2000; Ramos et al., 2002; Finzel et al., 2011; Gardner et al., 2013). Tectonic underplating of the slab and overlying off-scraped sediments may also contribute to uplift and exhumation (Fuis et al., 2008; Ducea et al., 2009).

Flat slab subduction is hypothesized to be the primary cause of modern orogenesis in southern Alaska (Plafker, 1987; Bruhn et al., 2004; Abers, 2008; Haeussler, 2008; Riccio et al., 2014). The driver for flat slab subduction is considered to be the Yakutat microplate, an exotic terrain consisting of an over-thickened (11–22 km) oceanic plateau that collides at 50 mm/yr into and subducts at a low angle beneath the North American plate (Figs. 1, 3; Plafker and Berg, 1994; Fletcher and Freymueller, 1999; Haeussler et al., 2003; Freymueller et al., 2008; Christeson et al., 2010; Elliott et al., 2010; Worthington et al., 2012). Flat slab subduction and associated collision in the St. Elias orogen initiated in the Middle Miocene (Plafker and Berg, 1994; Perry et al., 2009; Enkelmann et al., 2010). The leading edge of the Yakutat plate is now located ~250 km northwest of the subduction zone at ~150 km depth under central Alaska (Ferris et al., 2003). The western trailing edge of the Yakutat plate is situated underneath northern Kenai Peninsula today and bends alongside the down going Pacific plate (Figs. 1, 3; Eberhart-Phillips et al., 2006; Fuis et al., 2008). Flat subduction of the Yakutat plate drives convergent deformation and orogenesis for hundreds of kilometers throughout the overriding plate (Mazzotti and Hyndman, 2002; Bruhn et al., 2004). The effect of this deformation includes widespread acceleration of exhumation (Enkelmann et al., 2010; Spotila and Berger, 2010), basin inversion (Finzel et al., 2011; Ridgway et al., 2011), and cessation of subduction related volcanism since the Eocene (Pavlis and Roeske, 2007).

Although the effects of Yakutat subduction are clearly expressed in the central and southern Alaska mountain ranges that lie directly above it, including the St. Elias, Chugach, Tordrillo, Talkeetna, and Alaska

Ranges (Spotila and Berger, 2010; Arkle et al., 2013; Haeussler, 2008), the spatial and temporal characteristics of the transition to areas beyond the leading edge of the subducting microplate are not clear. Deformation related to the Yakutat plate has been suggested to penetrate 600–800 km northeast and 150–200 km northwest of the collision zone (Fig. 1; Mazzotti and Hyndman, 2002; Finzel et al., 2011). Evidence for this deformation is seen in basin inversion and faulting away from the immediate zone of Yakutat subduction (Pavlis and Roeske, 2007; Ridgway et al., 2007; Finzel et al., 2011; Haeussler and Saltus, 2011), but it is not fully understood how upper plate deformation decreases with distance from the subducting slab or what transitions occur at the margin of the slab. The Kenai Peninsula is an example of such a location that lies at the transitional zone just outside of Yakutat flat slab subduction.

2.2. The Kenai Peninsula

The Kenai Peninsula is a northeast trending forearc high situated along the transition from flat slab subduction of the Yakutat plate to normal subduction of the Pacific plate beneath southern Alaska (Fig. 1). The peninsula forms the westernmost component of a continuous arc of mountainous topography that extends as far east as the Fairweather Range (Buscher et al., 2008). The rugged Kenai Mountains are located along the peninsula south of the Turnagain Arm, and is the southwestern continuation of the Chugach Mountains to the northeast. Although the Kenai Mountains are situated to record the changes in deformation and rock uplift that occur at the edge of flat subduction, little is known about its recent deformational and denudational history.

The Kenai Peninsula is composed of the Cretaceous and early Tertiary Chugach and Prince William terranes and associated Tertiary–Neogene cover over the Jurassic terrane underlying the Kenai lowlands (Fig. 2). These terranes were accreted to the forearc in the Late Cretaceous to early Tertiary via motion on the Border Ranges and Contact faults (Freeland and Dietz, 1973; Plafker et al., 1989; Plafker and Berg, 1994; Haeussler et al., 2003; Fuis et al., 2008). The terranes were metamorphosed and intruded due to subduction of the Kula-Resurrection ridge from 57–52 Ma (Haeussler et al., 2003; Bradley et al., 2000). The Yakutat plate began subducting beneath the southern margin of Alaska by 32–23 Ma, and reached the forearc by Late Oligocene and Early Miocene (Plafker and Berg, 1994; Haeussler et al., 2003; Finzel et al., 2011). The uplift of the Kenai Peninsula may have been related to passage of the Yakutat plate beneath it. Sedimentary and stratigraphic relationships in Cook Inlet suggest that emergence and erosion of the Kenai Mountains began during the Miocene and became the predominant source of sediment by the Late Miocene (Kirschner and Lyon, 1973). The Beluga formation records the onset of widespread deposition from the Kenai Mountains and is characterized by conglomeratic sandstones and the presence of epidote which is uniquely characteristic of the Chugach terrane (Kirschner and Lyon, 1973). This timing roughly matches when the Yakutat microplate passed underneath the peninsula.

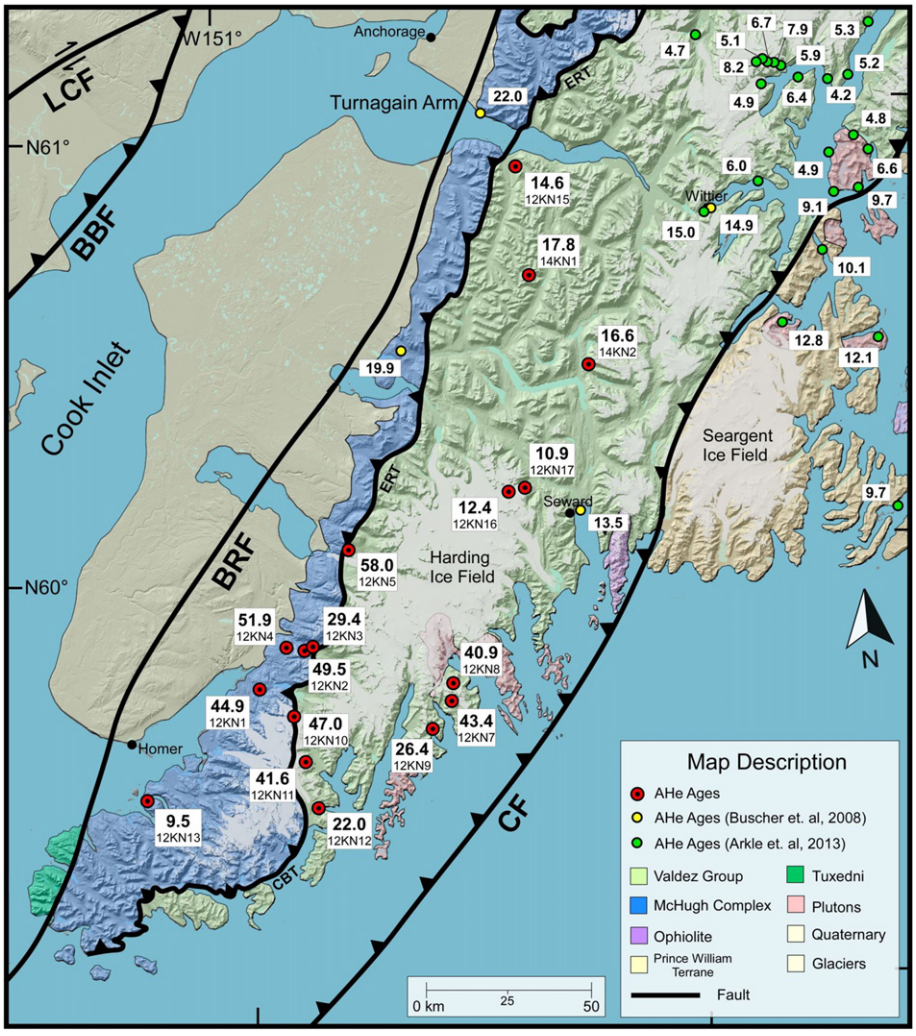

Fig. 2. AHe ages for the Kenai Peninsula (in Ma). Previously completed ages (green and yellow circles) from other studies are included along with 17 new AHe ages (red circles). BBF = Bruin Bay Fault, CF = Contact Fault, LCF = Lake Clark Fault.

The EDGE seismic transect between the Kenai Peninsula and Kodiak Island revealed an erosional backstop, where the accretionary prism is absent and older Eocene strata occur (Ye et al., 1997; Von Huene et al., 1998; von Huene and Klaeschen, 1999). This unconformity is interpreted to be related to the passage of the trailing edge or southwest margin of the Yakutat plate beneath the region, and stratigraphic relationships place the timing of this event at 3.5 Ma (Von Huene et al., 1998). The orientations and movements of the Yakutat and Pacific plates since 3.5 Ma have caused the trailing edge to migrate to the northeast underneath the Kenai Peninsula until it reached the present position under northernmost Kenai Peninsula and Sargent Ice field (Von Huene et al., 1998; Pavlis et al., 2004; Eberhart-Phillips et al., 2006).

Modern deformation of the Kenai Peninsula is associated with the Yakutat collision and Pacific Plate subduction (Haeussler et al., 2003). The axis of the peninsula lies ~250 km from the modern trench (Fig. 1). Farther north in the Chugach Mountains, which lie directly above the subducting Yakutat microplate, convergence is thought to have been primarily accommodated via thrusting and rock uplift on the Contact fault since the Mid-Miocene (Arkle et al., 2013). The role of the Contact fault in deformation along the Kenai Peninsula has not yet been defined. The Border Ranges fault is the other major fault in the region and is thought to act as the modern backstop to forearc deformation in the Chugach and Kenai Mountains (Plafker et al., 1989; Plafker and Berg, 1994; Arkle et al., 2013). The Border Ranges fault experienced dextral and contractional reactivation in the Neogene, but is buried by undeformed late Tertiary glacial deposits along the Kenai Mountains (Pavlis and Bruhn, 1983; Little and Naeser, 1989; Plafker et al., 1989; Plafker and Berg, 1994). Contractional deformation also occurs west of the Kenai Peninsula in the Cook Inlet. This forearc basin consists of a succession of Mesozoic and Cenozoic sediment, sourced from the surrounding mountains, that are 12 km- and 7 km-thick, respectively (Fisher and Magoon, 1978; Bruhn and Haeussler, 2006). Active shortening in the basin due to coupling along the megathrust ranges from 0.3 to 2.7 mm/yr and is manifest as a series of Pliocene to Quaternary anticlines and several mm/yr dextral and reverse slip along the Castle Mountain and Bruin Bay faults (Hartman et al., 1974; Cohen and Freymueller, 1997; Haeussler et al., 2000; Parry et al., 2001; Bruhn and Haeussler, 2006; Willis et al., 2007) (Fig. 3). This recent deformation has been attributed to a combination of the Yakutat collision to the east and subduction of the Pacific plate below the region (Haeussler et al., 2000).

Although sedimentary records in Cook Inlet suggest that the Kenai Mountains began eroding during the Late Miocene, the spatial pattern, magnitude, and rate of uplift and erosion are not constrained. The Kenai Mountains consists of a 150-km-long elliptical mountainous region that is the southern continuation of the coastal orogen (Fig. 3). The Kenai Mountains have an average height of ~2000 m asl and tapers gradually to the west, where it is juxtaposed by the Border Ranges

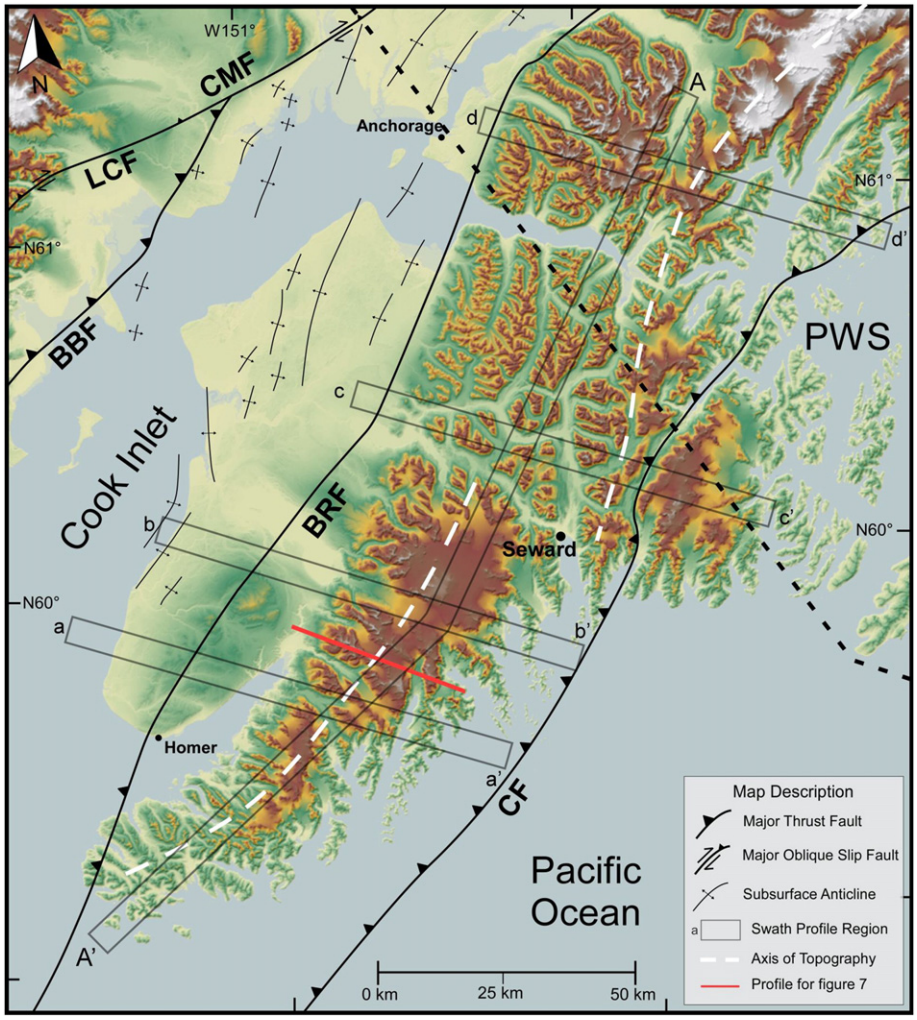

Fig. 3. A 300-m digital elevation model overlain with major faults and subsurface anticlines. Topography is similar in ruggedness to the Chugach Mountains (see text for details). The axis of the mountain range shifts to the west south of Seward. The dashed line represents the location of the subducted Yakutat slab beneath the region. Rectangles represent locations of swath profiles depicted in Fig. 4. BRF = Border Ranges Fault, BBF = Bruin Bay Fault, CMF = Castle Mountain Fault, CF = Contact Fault, LCF = Lake Clark Fault.

fault, causing an abrupt linear trend against the Cenozoic fill of Cook Inlet. On the east the range is dissected by glacial fjords, where cirques are submerged below sea level. The apparent subsidence on the east flank of the mountains is estimated to be ~100–300 m (Plafker, 1969) which may have been caused by a combination of rising sea level, climate changes during the LGM, and dynamic subsidence. The summits of the Kenai Mountains are heavily glaciated, capped by the Sargent and Harding icefields. These icefields give the range a welt-like appearance, as an elliptical concentration of high elevation that tapers off radially before merging with the Chugach Mountains (Fig. 4). Because of the presence of glaciers, mean slopes for Alaska mountain ranges are lower than expected based on the steepness of bare bedrock surfaces (Buscher et al., 2008). In the Kenai Mountains, for example, unglaciated surfaces above modern glacial trimline tend to be at or beyond the angle of repose. Nonetheless, the average slope in the Kenai Mountains (17°) is comparable to that observed in both the Chugach (19°) and St. Elias (16°) ranges, both of which lie directly over the Yakutat slab (Buscher et al., 2008; Arkle et al., 2013). The welt-like nature of the Kenai Mountains is also apparent in the geometry of drainage basins (Fig. 5). North of the Kenai Mountains, the main divide occurs near the eastern edge of the peninsula, whereas in the Kenai Mountains the divide steps west to the central axis of the peninsula and separates much smaller basins. The concentration of high elevation, relief, and glacial coverage into a welt in the Kenai Mountains suggests it may be a locus of rock uplift, similar to the bull's eye of rock uplift in the comparably rugged western syntaxis of the Chugach Mountains at the north end of Prince William Sound (Arkle et al., 2013).

Glacial climate and associated glacial and periglacial processes are probably a contributing factor to the ruggedness of the Kenai Mountains. The eastern side of the Kenai Peninsula experiences a wet maritime climate with ~180 cm/yr precipitation, whereas the western side experiences a colder continental interior climate with only ~50 cm/yr precipitation (National Climate Data Center, 2005, 2007). A result of this orographic gradient is heavier glaciation of the eastern flank, where glacial equilibrium line altitude (ELA) drops to ~800 m asl, whereas on the western flank ELA is above 1200 m asl (Péwé, 1975; Mann and Peteet, 1994; Wiles et al., 1995). During the local last glacial maximum, estimated to have been ~23 ka for this region (Karlstrom, 1961), the ELA was 300–500 m lower and glaciers covered the majority of the peninsula (Wiles et al., 1995). Based on the warm maritime setting, glaciers throughout the Quaternary on the Kenai Peninsula are likely to have been wet-based and therefore highly erosive (Péwé, 1975).

The exhumation history of the Kenai Mountains has not yet been documented because of a lack of previous low temperature thermochronometry in the coastal orogen (Fig. 1). However, previous work has defined the exhumation pattern of neighboring ranges. Apatite fission-track and (U–Th)/He ages from the Chugach and St. Elias ranges reveal rapid exhumation of >1 mm/yr and up to 5 mm/yr in the core of the Yakutat collision zone, tapering away to <0.1 mm/yr to the north and west (Spotila et al., 2004; Enkelmann et al., 2010; Spotila and Berger, 2010). Local concentrations of late Cenozoic exhumation of 0.4–0.5 mm/yr occur in a bull's eye of the western Chugach syntaxis at Mount Marcus Baker and along splay faults in Prince William Sound, including on the Patton Bay fault on Montague Island (Arkle et al., 2013; Ferguson et al., 2015; Haeussler et al., 2015). These exhumation hotspots decay to average rates of <0.05 mm/yr in the Chugach Mountains and northern portion of the Kenai Peninsula (Buscher et al., 2008). Testing whether a hotspot of exhumation occurs in the Kenai Mountains and relating this exhumation to regional tectonics are the main goals of this study.

3. Methods

Low temperature thermochronometry was used to constrain the exhumation history of the Kenai Mountains. We obtained seventeen new apatite AHe ages across the region, where no previous low temperature thermochronometry had been completed. Sample locations were broadly distributed to provide regional spatial coverage, although locally samples were clustered to provide a range of elevation. However, rugged terrain prevented the collection of good vertical sample profiles. Samples were collected via helicopter and where trail access was possible. AHe ages are based on the radiogenic production and thermal diffusion of ^{4}He and record cooling from closure temperatures of ~50–70 °C,

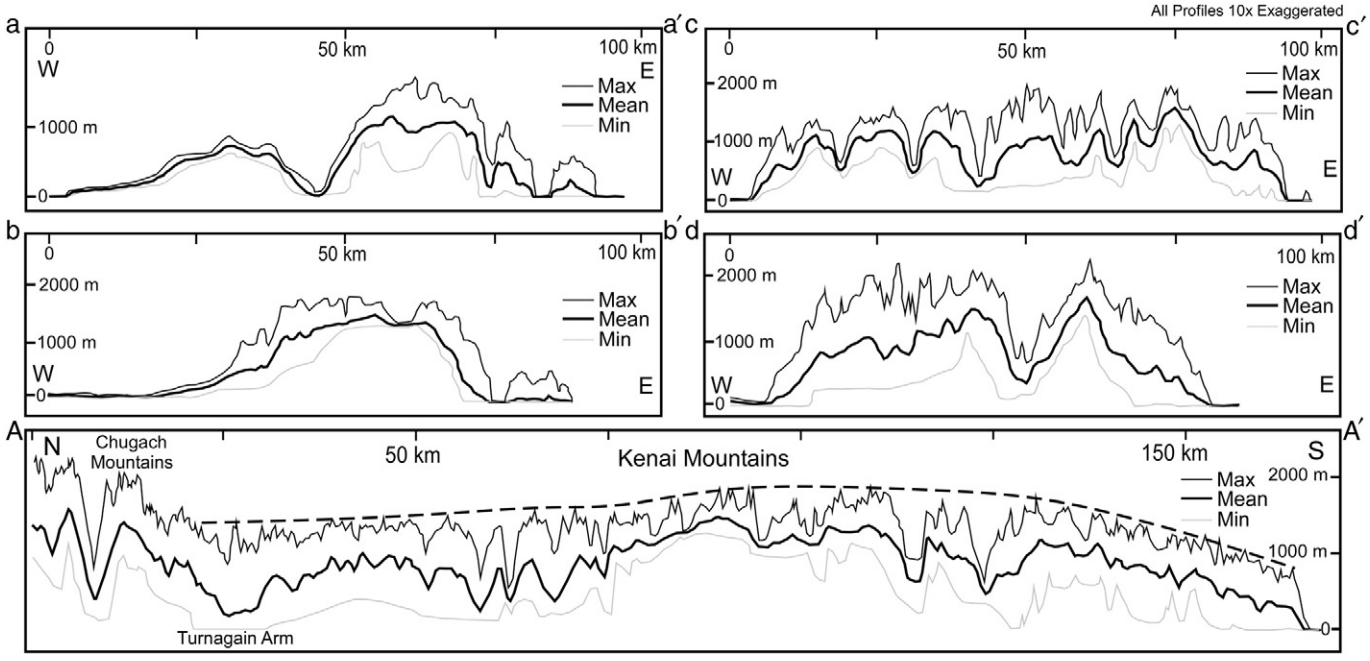

Fig. 4. Swath profiles depicting topography across the Kenai Peninsula (a–d) and a long axis profile (A–A′)down the Kenai Peninsula. See Fig. 3 for the locations of the profiles. Profiles a–a′ and b–b′ show the dome like topography of the Harding Icefield and the southern half of the Kenai Peninsula. Profile c–c′ shows the unglaciated portion of the northern Kenai Peninsula. Profile d–d′ shows the higher and more deeply incised topography of the Chugach Mountains to the north. Profile A–A′ shows the distinct topographic characteristics that separate the Kenai Mountains from the Chugach Mountains and the concordant elevation of peaks and ridges (black dashed line).

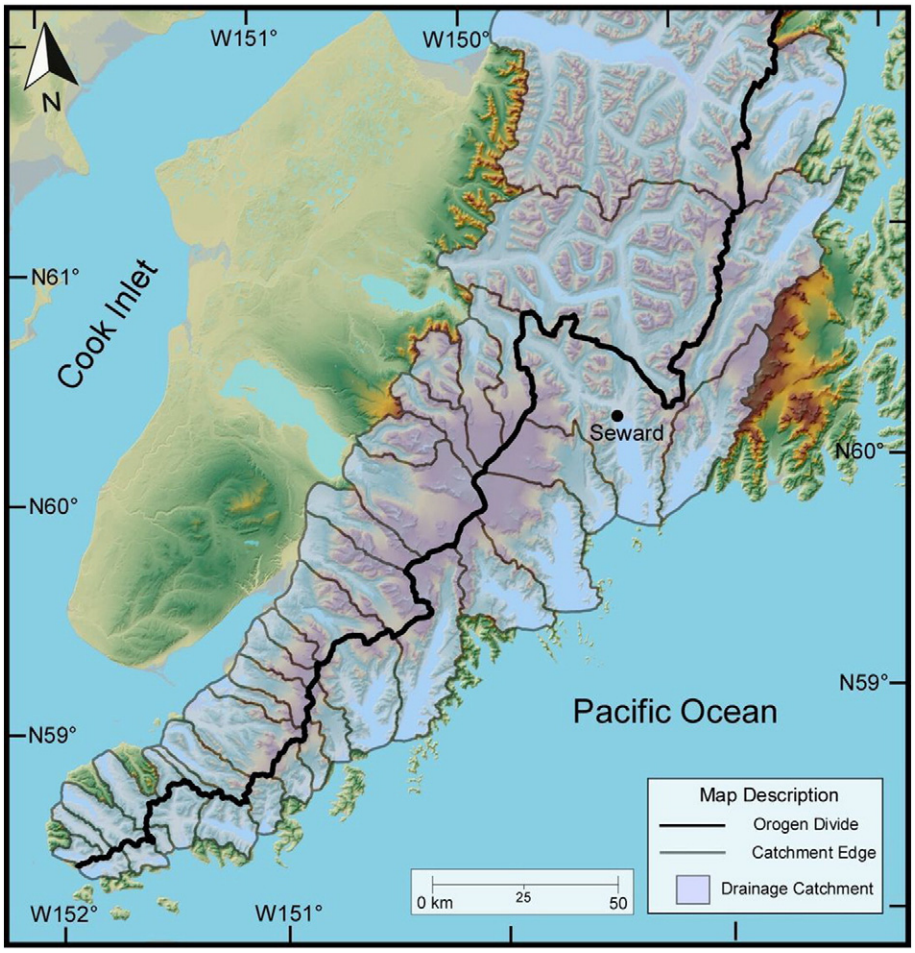

Fig. 5. A 300-m digital elevation model of the Kenai Peninsula showing the main drainage divide and individual catchments. The drainage divide follows the coast to the north, but steps west south of Seward. Similarly, the drainage catchments are large (1600 km^2) north of Seward and substantially smaller (300 km^2) to the south.

or exhumation from ~2–3 km depth for typical geothermal gradient (i.e. 25 °C) (Farley, 2000; Ehlers and Farley, 2003). Closure temperatures for AHe are dependent on multiple factors, however, including cooling history, crystal grain size, and radiation damage (Farley, 2000; Ehlers and Farley, 2003; Flowers et al., 2009; Brown et al., 2013).

AHe ages were measured at Virginia Tech on both single and multi-grain aliquots. Dated apatite grains were generally >70 μm in diameter and were selected under 100× magnification based on distinct crystal habit, birefringence, relief, and lack of obvious microinclusions or fractures. Aliquots were outgassed in Pt tubes in a resistance furnace at 950 °C for 20 min and analyzed for ^{4}He by ^{3}He spike and quadrupole mass spectrometry. Radiogenic parent isotopes were measured at the University of Arizona using isotope dilution and ICP mass spectrometry. Predicted age uncertainty is ~5% (1σ), based on instrument precision and F_T calculations (Farley, 2000). However, average observed standard deviation of measured ages was 19.5% (1σ) (Table 1). In addition, 19 outlier age determinations (17% of total) were culled from the data set prior to the calculation of mean ages, on the basis that they were more than double the mean age and thus likely anomalous (Table 1). Comparably large uncertainties have been observed in other nearby studies (11–17%, 1σ) (Buscher et al., 2008; Arkle et al., 2013; Ferguson et al., 2015), suggesting that local lithologies (graywacke, metaflysch) are problematic for AHe dating. For this reason, we took the approach of Berger et al. (2008) and measured a high number of replicate analyses per sample (~6, but as high as n = 13) to improve reproducibility.

Several samples (12Kn7, 12Kn8, 12Kn12) had particularly poor reproducibility that seems to relate to poor apatite quality, crystal grain size, and abundance. Fig. 6 shows example apatite grains and lithologies that are representative of these samples. Reasonable quality apatite occurred in some samples that are typical of other studies (A and B in Fig. 6). In contrast, many of the apatites were opaque, broken along their basal cleavage, i.e., parallel to 001 plane, or fractured (C–G in Fig. 6). The surfaces of many grains were also frosted, etched, or rounded, possibly associated with sedimentary transport and post-burial alteration. Anomalously old ages may result from the presence of radiogenic microinclusions that went undetected in these visually imperfect grains. Observed age dispersion may also result from the occurrence of fractures or other crystal imperfections, which introduce the possibility for loss of ^{4}He, loss of parent radiogenic material, and complications in correctly measuring F_T values (Brown et al., 2013). Differences in chemistry, parent atom zonation, and radiation damage are other potential causes of age dispersion (Flowers et al., 2009), particularly given that our samples are sedimentary or metasedimentary in origin and thus consist of multi-sourced detrital apatite. Rough positive correlations between eU and AHe age for several samples suggest that radiation damage could be a contributing factor to the observed age dispersion. However, a surprising result of this study is that measured ages on large, fractured, opaque single grain with microinclusions, which traditionally would have been avoided, reproduced reasonably well (H and I in Fig. 6).

4. Results

The range of measured AHe ages in the Kenai Mountains is ~10–58 Ma (Fig. 2). These ages are relatively old in comparison to other studies in southern Alaska (e.g. Spotila and Berger, 2010; Arkle et al.,

Table 1
AHe data.

Sample	Elevation (m)	Latitude	Longitude	Rock type	Mass (mg)	mwar (μm)	He (pmol)	U (ppm)	Th (ppm)	Sm (ppm)	eU	Grains	F_T	Corr. age (Ma)	Average age (Ma)	Standard deviation
12KN1	713	59.7295	−150.8627	Meta. sand	0.0013	46.0	0.0022	8.3	16.4	141.6	12.8	1	0.68	40.1	**44.9**	8.5 Ma
					0.0018	50.6	0.0010	3.3	6.3	60.0	5.1	1	0.79	28.1	n = 8**	19.0%
					0.0022	32.2	0.0033	5.3	14.6	127.2	9.4	3	0.63	50.5	N = 8***	
					0.0137	47.2	0.0201	4.9	10.3	101.6	7.8	5	0.74	50.1		
					0.0065	69.0	0.0097	5.1	7.8	115.8	7.5	1	0.82	48.2		
					0.0044	55.2	0.0108	7.1	22.1	117.2	12.9	1	0.76	48.4		
					0.0111	46.4	0.0182	5.3	10.3	145.9	8.5	5	0.72	54.5		
					0.0113	38.0	0.0411	20.2	24.4	164.6	26.8	12	0.67	39.4		
12KN2	1227	59.8524	−150.6686	Graywacke	0.0023	64.4	0.0034	5.1	9.3	121.4	7.9	1	0.81	45.6	**49.5**	3.8 Ma
					0.0029	55.2	0.0037	4.1	9.3	115.7	6.9	1	0.81	46.6	n = 6	7.7%
					0.0052	59.8	0.0069	4.3	9.0	153.0	7.2	1	0.80	47.1	N = 6	
					0.0066	69.0	0.0086	3.8	6.3	152.0	6.1	1	0.81	55.4		
					0.0042	53.0	0.0076	5.4	12.6	161.2	9.2	2	0.76	52.5		
					0.0033	48.5	0.0051	4.7	13.5	183.8	8.8	4	0.71	49.7		
12KN3	1568	59.8607	−150.6456	Graywacke	0.0051	69.0	0.0274	29.7	43.3	107.8	40.4	1	0.82	31.1	**29.4**	2.3 Ma
					0.0044	*52.2*	*0.0059*	*3.8*	*10.8*	*146.6*	*7.1*	*2*	*0.76*	*50.7*	n = 2	8.0%
					0.0080	*42.5*	*0.0366*	*14.7*	*8.0*	*279.5*	*18.0*	*7*	*0.69*	*74.3*	N = 4	
					0.0077	35.9	0.0197	21.3	22.5	215.0	27.7	7	0.65	27.7		
					0.0138	*75.6*	*0.0352*	*2.1*	*6.1*	*118.2*	*4.1*	*2*	*0.83*	*223*		
12KN4	99	59.8524	−150.7424	Graywacke	0.0055	34.7	0.0057	3.7	8.8	166.9	6.7	5	0.63	50.9	**51.9**	7.4 Ma
					0.0057	36.8	0.0054	3.9	9.2	138.4	6.8	5	0.66	43.2	n = 5	14.3%
					0.0060	*37.7*	*0.0181*	*4.2*	*9.7*	*146.6*	*7.2*	*5*	*0.66*	*130*	N = 6	
					0.0058	35.3	0.0070	4.4	10.8	162.4	7.7	6	0.63	50.6		
					0.0074	39.1	0.0112	4.3	9.6	169.3	7.4	6	0.66	63.8		
					0.0053	38.0	0.0094	6.2	14.8	197.0	10.6	5	0.67	50.7		
12KN5	1141	60.0678	−150.4240	Meta. sand	0.0030	39.8	0.0246	22.8	42.3	120.1	33.3	3	0.68	70.0	**58.0**	13.0 Ma
					0.0091	78.2	0.0698	24.1	20.2	34.1	29.0	1	0.84	59.8	n = 3	22.4%
					0.0102	*101.2*	*0.3968*	*24.0*	*7.4*	*210.2*	*26.8*	*1*	*0.90*	*312*	N = 4	
					0.0039	70.1	0.0010	1.2	0.4	42.3	1.5	2	0.83	44.1		
12KN7	598	59.7393	−150.0264	Meta. sand	0.0051	73.6	0.0128	5.6	12.6	219.1	9.6	1	0.86	62.5	**43.4**	14.3 Ma
					0.0087	71.6	0.0292	8.7	17.1	183.7	13.6	2	0.82	59.6	n = 10	32.9%
					0.0068	47.7	0.0210	41.1	22.6	194.5	47.4	3	0.77	16.4	N = 10	
					0.0061	64.4	*0.0001	0.1	0.5	6.6	0.3	1	0.81	24.0		
					0.0070	82.8	*0.0002	0.3	0.1	16.1	0.4	1	0.85	40.2		
					0.0077	87.4	0.0418	18.9	21.6	148.3	24.8	1	0.85	49.6		
					0.0128	101.2	0.0022	0.7	0.2	30.1	0.9	1	0.90	46.5		
					0.0079	52.8	0.0169	5.9	17.3	205.2	10.9	2	0.80	49.6		
					0.0035	55.4	0.0105	10.6	20.9	242.9	16.7	2	0.81	44.1		
					0.0044	68.8	0.0220	19.4	37.7	213.2	29.4	2	0.82	40.9		
12KN8	10	59.7685	−150.0314	Meta. sand	*0.0152*	*105.8*	*0.0064*	*0.9*	*0.3*	*3.8*	*1.0*	*1*	*0.88*	*93.8*	**40.9**	11.7 Ma
					0.0099	76.4	0.0810	45.7	17.1	135.9	50.4	2	0.82	38.0	n = 8	28.7%
					0.0096	54.3	0.1408	73.7	8.4	197.5	76.6	3	0.78	47.4	N = 10	
					0.0130	*49.6*	*0.2988*	*42.5*	*5.5*	*127.4*	*44.4*	*8*	*0.73*	*136*		
					0.0059	37.8	0.0589	52.6	7.3	179.0	55.2	4	0.68	51.6		
					0.0137	51.3	0.0058	6.0	1.3	39.4	6.5	6	0.74	17.1		
					0.0209	147.2	0.0194	4.4	0.6	35.1	4.7	1	0.93	42.1		
					0.0054	51.4	0.0348	30.9	6.3	143.4	33.1	3	0.77	49.7		
					0.0125	80.1	0.0213	11.3	2.4	28.1	12.0	2	0.86	31.8		
					0.0130	70.1	0.1225	42.3	4.0	143.8	44.0	2	0.84	49.5		
12KN9	1	59.6333	−150.0969	Schist	*0.0015*	*48.5*	*0.0151*	*47.6*	*47.4*	*186.2*	*59.6*	*3*	*0.74*	*45.3*	**26.4**	1.5 Ma
					0.0087	72.8	0.0418	36.5	17.5	174.6	41.5	2	0.82	27.3	n = 4	5.7%
					0.0027	*51.0*	*0.0099*	*6.8*	*16.6*	*184.3*	*11.6*	*2*	*0.75*	*85.5*	N = 7	
					0.0082	52.1	0.0281	24.7	33.3	168.5	33.4	2	0.80	24.8		
					0.0088	*92.0*	*0.0003	*1.1*	*0.2*	*12.2*	*1.2*	*1*	*0.86*	*6.70*		
					0.0062	55.2	0.0254	31.5	34.1	103.1	40.1	2	0.78	25.4		
					0.0045	53.2	0.0198	27.3	49.2	196.3	39.8	2	0.77	28.0		
12KN10	375	59.7330	−150.7876	Graywacke	0.0091	82.8	0.0059	1.6	6.0	191.1	4.0	1	0.87	43.1	**47.0**	3.1 Ma
					0.0070	78.2	0.0236	11.5	25.9	183.4	18.5	1	0.85	42.0	n = 9	6.6%
					0.0048	61.3	0.0090	5.2	16.8	175.5	10.0	2	0.80	46.8	N = 9	
					0.0046	49.0	0.0069	5.1	12.3	150.4	8.7	2	0.75	46.1		
					0.0051	73.6	0.0153	8.9	20.8	191.7	14.7	1	0.83	48.4		
					0.0046	55.2	0.0097	6.2	18.1	220.3	11.6	2	0.79	47.1		
					0.0086	67.6	0.0172	6.0	15.3	182.4	10.5	2	0.83	46.6		
					0.0072	59.8	0.0127	4.2	16.3	131.3	8.7	2	0.80	50.9		
					0.0055	57.8	0.0109	5.0	16.7	161.5	9.7	2	0.79	51.5		
12KN11	820	59.6727	−150.7210	Meta. sand	0.0083	51.5	0.0271	11.6	35.4	280.1	21.3	5	0.76	40.4	**41.6**	1.6 Ma
					0.0058	43.7	0.0101	5.2	24.9	151.4	11.8	5	0.69	42.7	n = 2/N = 2	4.0%
12KN12	602	59.5215	−150.6630	Meta. sand	0.0111	124.2	0.0353	12.6	51.2	296.3	26.1	1	0.88	27.0	**22.0**	5.8 Ma
					0.0140	72.3	0.0185	10.0	14.6	201.8	14.5	4	0.83	21.9	n = 11	26.4%
					0.0075	92.0	0.0155	53.8	1.5	242.8	55.4	1	0.86	8.41	N = 13	
					0.0122	*56.7*	*0.4918*	*29.4*	*31.7*	*298.0*	*38.4*	*4*	*0.77*	*262*		
					0.0074	71.8	0.0209	18.4	28.1	242.0	26.2	3	0.83	25.7		

(continued on next page)

Table 1 (*continued*)

Sample	Elevation (m)	Latitude	Longitude	Rock type	Mass (mg)	mwar (μm)	He (pmol)	U (ppm)	Th (ppm)	Sm (ppm)	eU	Grains	F_T	Corr. age (Ma)	Average age (Ma)	Standard deviation
					0.0057	40.5	0.0027	4.2	17.3	209.0	9.3	4	0.68	15.6		
					0.0042	69.0	0.0031	4.4	11.1	257.1	8.3	1	0.82	23.0		
					0.0061	*52.8*	*0.1312*	*5.0*	*13.4*	*234.4*	*9.3*	*4*	*0.77*	*611*		
					0.0017	39.7	0.0050	24.6	31.1	248.2	33.2	3	0.68	25.2		
					0.0046	50.4	0.0046	4.9	17.1	238.2	10.1	3	0.75	27.1		
					0.0090	72.8	0.0162	12.0	22.5	214.0	18.3	3	0.82	23.6		
					0.0015	39.4	0.0283	288.1	63.8	309.8	304.7	4	0.67	18.4		
					0.0052	78.2	0.0185	23.4	27.6	266.4	31.2	1	0.84	26.4		
12KN13	657	59.5260	−151.3715	Graywacke	0.0093	82.8	0.0053	16.3	1.8	146.5	17.5	1	0.85	7.53	**9.5**	2.5 Ma
					0.0084	78.2	0.0061	18.0	3.6	147.6	19.5	1	0.84	8.71	n = 3	26.4%
					0.0069	73.6	0.0066	18.0	1.4	154.8	19.1	1	0.80	12.3	N = 3	
					0.0117	*39.9*	*0.0432*	*27.9*	*9.5*	*220.7*	*31.2*	*11*	*0.68*	*34.0*		
12KN15	94	60.9093	−149.6064	Meta. sand	0.0057	64.4	0.0027	7.3	16.9	131.2	12.0	1	0.80	9.88	**14.6**	3.4 Ma
					0.0068	69.0	0.0028	5.2	9.7	201.0	8.5	1	0.82	12.1	n = 5	23.3%
					0.0067	78.2	0.0037	5.9	7.4	90.8	8.1	1	0.81	16.5	N = 6	
					0.0114	101.2	0.0202	15.4	25.7	239.9	22.6	1	0.87	17.7		
					0.0129	*52.3*	*0.0243*	*15.4*	*21.2*	*104.0*	*20.9*	*5*	*0.75*	*23.2*		
					0.0083	40.0	0.0206	30.8	45.2	154.4	42.2	6	0.68	16.6		
12KN16	1076	60.1800	−149.7063	Meta. sand	0.0137	45.9	0.0283	41.4	36.3	207.3	51.0	6	0.72	10.8	**12.4**	1.1 Ma
					0.0057	92.0	0.0117	21.2	55.2	245.7	35.4	1	0.86	13.2	n = 6	9.2%
					0.0085	62.2	0.0106	13.8	33.7	231.4	22.9	2	0.80	13.4	N = 6	
					0.0052	55.2	0.0088	19.9	51.0	255.3	33.2	2	0.78	12.7		
					0.0073	47.4	0.0091	15.1	40.1	187.9	25.4	6	0.72	13.1		
					0.0132	41.2	0.0342	51.5	54.8	179.7	65.2	9	0.69	11.0		
12KN17	103	60.1947	−149.5880	Meta. sand	0.0033	73.6	0.0074	21.9	43.8	237.5	33.4	1	0.83	15.8	**10.9**	2.4 Ma
					0.0026	46.0	0.0040	22.0	45.8	68.9	33.1	1	0.74	12.1	n = 7	22.6%
					0.0039	39.6	0.0044	23.2	39.2	262.7	33.7	2	0.74	8.96	N = 10	
					0.0041	43.2	0.0058	24.8	47.4	136.8	36.6	3	0.71	10.4		
					0.0066	87.4	0.0011	1.9	4.7	191.5	4.0	1	0.88	10.5		
					0.0029	59.8	0.0011	6.5	13.4	236.5	10.8	1	0.78	9.26		
					0.0033	47.1	0.0020	13.7	12.8	92.0	17.1	2	0.76	8.99		
					0.0030	*39.3*	*0.0096*	*6.0*	*10.7*	*154.2*	*9.3*	*2*	*0.69*	*99.3*		
					0.0032	*59.8*	*0.0093*	*16.8*	*31.5*	*175.9*	*25.1*	*1*	*0.82*	*27.0*		
14KN1	1249	60.6582	−149.5311	Meta. sand	0.0062	62.3	0.0131	15.4	23.1	174.5	21.7	2	0.80	23.8	**17.8**	5.3 Ma
					0.0054	64.1	0.0139	34.5	33.8	153.2	43.2	2	0.82	13.9	n = 3	29.9%
					0.0054	59.7	0.0037	7.1	15.0	94.1	11.1	2	0.79	15.4	N = 3	
14KN2	1459	60.4523	−149.2947	Schist	0.0222	147.2	0.0394	30.1	9.2	41.9	32.4	1	0.93	11.3	**16.6**	7.4 Ma
					0.0077	69.5	0.0163	13.9	33.7	73.7	22.2	2	0.83	21.8	n = 2	44.8%
															N = 2	

meta. = metamorphic rock.
sand = sandstone.
mwar = mass-weighted average radius.
FT = alpha ejected correction factor.
eU = U + (0.235 * Th), effective uranium concentration.
Standard deviation of ages used for average are as Ma and percent.
Ages in italics are excluded from averages (see text for explanation).
Latitude and longitude datum is WGS84 and vertical datum is EGM96.
* Measured ^{4}He was low and corresponds to higher uncertainty.
** "n" = number of replicates used in age.
*** "N" = total number of aliquots run for age.

2013; Ferguson et al., 2015) and are not indicative of recent, rapid exhumation. The "bull's eye" of young (<5 Ma) AHe ages identified north of Prince William Sound (Arkle et al., 2013), for example, does not extend southwards into the Kenai Mountains, despite the rugged topography of the range that would suggest recent uplift and erosion.

Ages in the north, closest to the Chugach Mountains, are the youngest measured (10–20 Ma). These ages overlap with those determined by Buscher et al. (2008); Arkle et al. (2013) and are relatively consistent across the entire Chugach Mountains from the Cook Inlet to Prince William Sound. Ages increase to 30–50 Ma in the central and southern Kenai Mountains. The ages are generally 40–50 Ma on the west and ~25 Ma on the Pacific coast (Fig. 7A). This trend is consistent with observations by Buscher et al. (2008) farther north in the Chugach Mountains, which are interpreted to represent an AHe partial retention zone that was tilted up on the east via greater exhumation along the Pacific coast. However, existing sample coverage does not permit a unique characterization of AHe isochron geometry. Likewise, sample coverage does not permit determination of age-elevation relationships. The few samples that do span a range of relief in close proximity to each other do not indicate an obvious age-elevation trend.

Although measured ages become younger to the southeast towards the Contact fault, they do not bear any other obvious relationship to mapped faults. However, one measured age may require a local tectonic explanation. Sample 12Kn13 from the southern part of the peninsula produced a younger age (9.5 Ma) that does not fit with the regional pattern (Fig. 2). Given that only one sample in the region shows this young age, however, we consider it to be an unexplained local phenomenon and additional data would be required to understand its significance.

The old AHe ages measured in this study are older than any ages previously measured in southern Alaska. The older ages measured in this study roughly correlate with the early Cenozoic ages measured previously in the Tordrillo Mountains (Haeussler, 2008). The three oldest ages in the Tordrillo Mountains (39, 48, and 74 Ma) were shown to be affected by apatite zonation, but these ages may also represent a slow background exhumation rate, similar to the older ages in the Kenai Mountains. The older AHe ages from the Kenai Mountains overlap

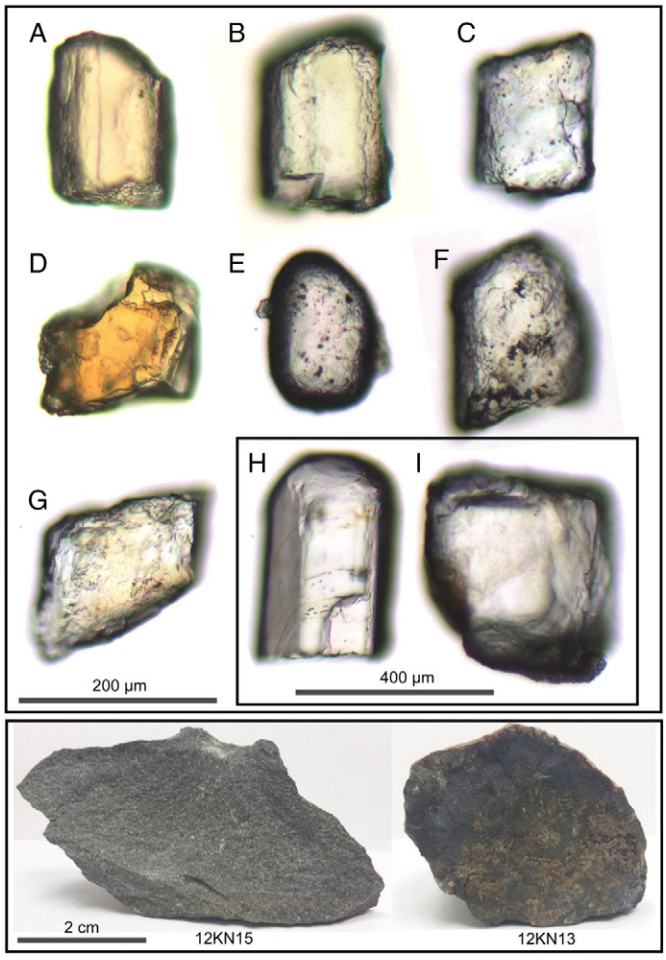

Fig. 6. Apatite grains and hand samples depicting the range of samples used for analysis in this study. Apatite grain A is an example of some of the best quality grains used for the study, but this quality was rare. Apatite grains B and C are broken and have imperfections on their surfaces, but still preserve crystal habit and are inclusion free. Apatite grain D is good quality but fractured on many of the edges. Apatite grain E has worn edges and is rosted, suggesting that it may have undergone transport and alteration before deposition. Apatites grains F and G are examples of some of the lowest quality apatites used for this study. Apatite grains Hand I are decent quality grains which are larger than >100 μm and were used as single grain aliquots, but grains such as these often had internal flaws and non-birefringent microinclusions. Hand sample 12KN15 is an example of a coarser grained metasandstone that yielded apatite. Sample 12KN13 is an example of the majority of samples for the Kenai Mountains, which is fine grained and produced low quality apatite.

with higher temperature cooling ages that suggest widespread rapid cooling post ~52 Ma (Helwig and Emmet, 1981; Bradley et al., 2000). This cooling event corresponds to a subduction of a slab window around ~55 Ma (Bradley et al., 2000). Our ages suggest that cooling to apatite closure temperatures must have been very rapid following this event. Since this cooling event, the upper crust must have been relatively stable and only slowly exhumed, allowing formation of a partial retention zone (PRZ).

5. Discussion

Despite its rugged topography, the Kenai Mountains do not appear to contain a locus of recent, rapid exhumation. Measured AHe cooling ages of 40–55 Ma are the oldest that have been measured along the coastal orogen of south-central Alaska. These ages imply that rocks of the Kenai Peninsula must have cooled quickly after passage of a slab window in early Cenozoic (Bradley et al., 2000), but subsequently experienced minimal exhumation and prolonged crustal stasis. Based on the oldest cooling age, a calculated closure temperature of ~58 °C, and an assumed geothermal gradient of ~22 °C/km calculated from the temperature logs of COST No. 1 well in Cook Inlet (Magoon, 1986), the average exhumation rate since 50 Ma has only been ~0.05 mm/yr, although we do not expect that exhumation would have been constant throughout the Cenozoic. An alternative explanation for the observed AHe ages is that the geothermal gradient in the forearc is lower than implied by Magoon (1986). Subduction refrigeration can accompany flat slab subduction, in which the cold down-going slab cools the overlying mantle wedge and decreases geothermal gradient by as much as 10–15 °C/km (Dumitru et al., 1991; Peacock, 1996; Westaway, 2006). If the geothermal gradient was much reduced following passage of a slab window beneath the Kenai Mountains, this could have rendered the AHe system insensitive to subsequent exhumation of even several kilometers. Without independent constraints on the mid to late Cenozoic geothermal gradient, however, this possibility is difficult to assess. We therefore elect to interpret our data using the best known estimate of current geothermal gradient (Magoon, 1986), while acknowledging the caveat that a lower than expected geothermal gradient could account for some of the spatial variation and great antiquity of the observed ages.

Although future work will be required to better determine age-elevation relationships in the area, the high variation in old AHe ages across minimal elevation range implies the occurrence of an AHe PRZ in the Kenai Mountains. The spatial variation in ages can be loosely fit by closely stacked isochrons of a PRZ that is tilted gently down to the west away from the windward side of the range (Fig. 7B). The orientation and location of the isochrons are difficult to define and non-unique, due to differences in sample elevation and scatter in the AHe ages. The crustal section containing this potential PRZ is less deeply eroded than the PRZ in the Chugach Mountains in the vicinity of Turnagain Arm, where ages are slightly younger (10–20 Ma) (Buscher et al., 2008). In regional context, it therefore appears that the locus of rapid exhumation in the Chugach Mountains north of Prince William Sound identified by Arkle et al. (2013) transitions gradually to a zone of moderate exhumation in the westernmost Chugach Mountains and to a zone of minimal exhumation farther southwest into the Kenai Mountains (Fig. 8). The transition from moderate to minimal exhumation near Seward is sharp and may represent the progressive change from the trailing edge of the Yakutat plate to the Pacific plate.

If the crest of the Kenai Mountains has experienced minimal erosion, the shape of the topography itself should represent the geometry of surface uplift responsible for creating the range. Topographic profiles show that the Kenai Mountains are a broad dome (Fig. 4). The dome has a sharp, fault-bounded western margin. Total recent exhumation into this dome has been limited to valley incision, without lowering of upper ridge surfaces. In the northern Kenai Mountains the dome is deeply incised, whereas in the south the dome is capped by the Harding Icefield. Across the dome the elevation of peaks and ridges are somewhat concordant and can be used to define an imaginary surface that represents the limit of recent rock uplift (Fig. 4) (Buscher et al., 2008). This dome could be produced as doubly-plunging antiformal arc of rock uplift. If correct, this interpretation suggests that the Kenai Mountains are a transient landform with erosion that lags behind surface uplift and creation of topographic potential energy (e.g. Ouimet et al., 2009; Oskin and Burbank, 2005). The Kenai Mountains may thus provide an example of a range in the early stage of orogenesis that is in a state of disequilibrium with the local erosional setting. A minor influence of climate on exhumation pattern may be apparent in the Kenai Mountains, however. The decrease in AHe age to the southeast and implied greater depth of erosion into the PRZ of ~0.5–1.0 km may be due to heavier precipitation and lower glacial ELA on the Pacific Coast (Fig. 7B).

Several lines of evidence combine with the relatively old AHe ages of the Kenai Mountains to suggest that they are kinematically distinct from the Chugach Mountains to the north. The gross topography of the Kenai Mountains appears disconnected and offset from the core of

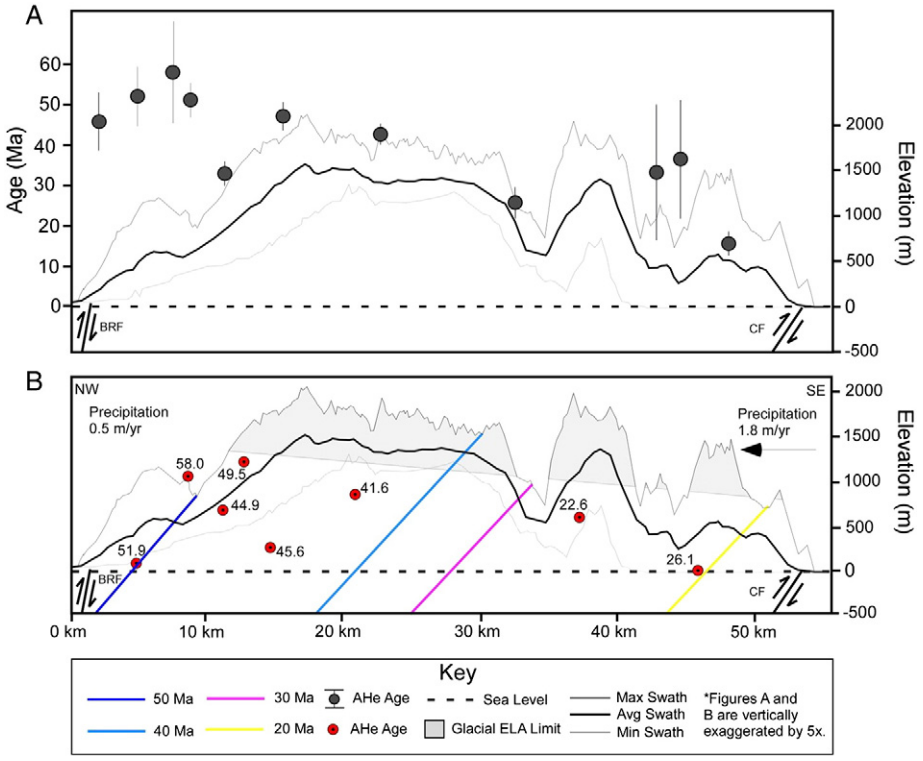

Fig. 7. (A) AHe age vs. distance along swath topographic profiles along the Kenai Mountains. The general trend of AHe ages shows a decrease towards the east and windward flank of the mountains. (B) Age distance plot with approximate AHe isochrons illustrating a potential PRZ tilted down to the west. Glacial ELA (Mann and Peteet, 1994; Wiles et al., 1995) is shown lowering towards the east due to precipitation gradient. BRF = Border Ranges Fault, CF = Contact Fault.

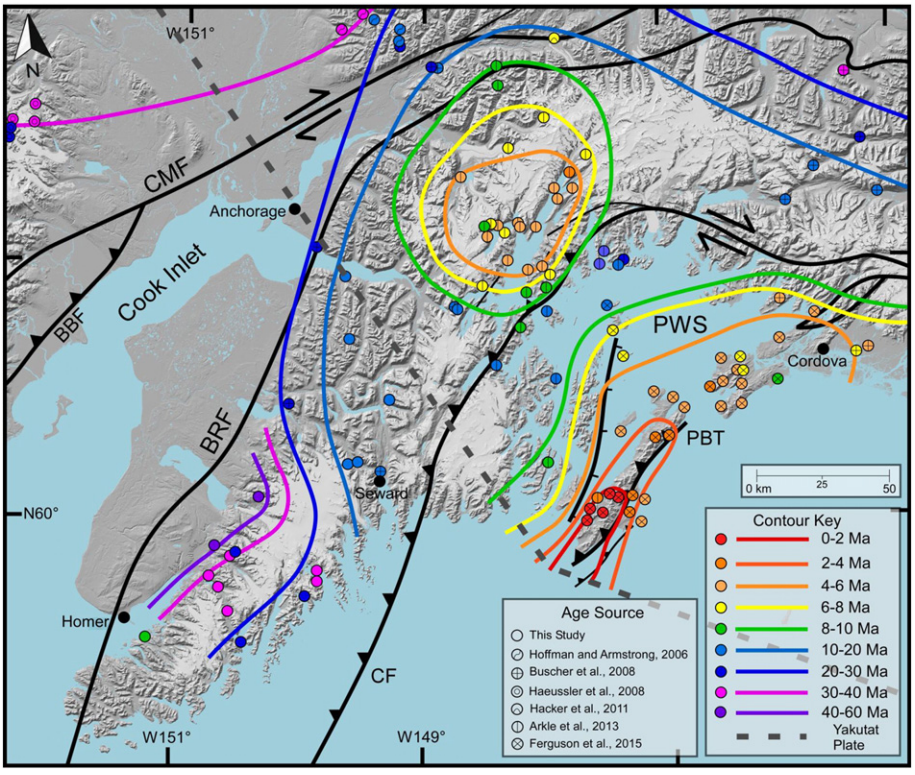

Fig. 8. AHe age contour map for the Prince William Sound and surrounding coastal mountains. The new AHe ages are the oldest in the region and portray a zone of slow exhumation southwest of the edge of the Yakutat plate. The Chugach Core and the Patton Bay Thrust regions have much faster exhumation rates due to upper plate deformation related to the Yakutat plate. BRF= Border Ranges Fault, BBF= Bruin Bay Fault, CMF = Castle Mountain Fault, CBT = Chugach Bay Thrust, CF= Contact Fault (Bol and Roeske, 1993), ERT = Eagle River Thrust, PBT = Patton Bay Thrust.

the Chugach Mountains at the southern margin of the underthrusting Yakutat microplate. The main drainage divide and axis of highest topography in the Kenai Mountains are situated in the center of the peninsula, whereas north of Seward in the Chugach Mountains the divide and topographic axis are located near the eastern margin of the mountains close to Prince William Sound, corresponding to much larger western catchments and glacial valleys (Figs. 3 and 5). The topographic crest jumps approximately 30 km to the west south of Seward and also changes orientation from north-south in the Chugach Mountains to NE–SW in the Kenai Mountains (Fig. 3). Greater erosion in the Chugach Mountains may have pushed the regional drainage divide to an axis of uplift in Prince William Sound near active faults like the Contact fault (Arkle et al., 2013). The locus of rock uplift in the Kenai Mountains may instead be focused in the middle of the peninsula, or a lower degree of erosion may have so far left the master divide in the Kenai Mountains immune to lateral shifts related to faulting, precipitation gradient, or glacier headward retreat. These transitions correspond to physical trends in the neighboring Cook Inlet. A shallowing of basin thickness to the south and increase in gravity anomalies roughly coincides with where AHe ages increase to the southwest of Seward (Mankhemthong et al., 2013).This suggests the tectonic rock uplift of the Kenai Mountains and deformation and subsidence in Cook Inlet may be related to each other, yet distinct from the deformation and uplift of the Chugach Mountains to the north.

Although it is possible that the deformation associated with flat slab subduction that is observed in the Chugach Mountains (Arkle et al., 2013) gradually tapers off with distance from the underthrusting plate, the transitions in exhumation and topography around Seward (Fig. 3), within the transition zone of slab dip from flat to normal subduction, suggest a fundamental change in tectonic origin of forearc deformation. An alternative explanation for uplift of the Kenai Mountains other than from the underthrusting Yakutat microplate is underplating along the Aleutian megathrust. Underplating along a subduction zone occurs when subducting sediment and oceanic crust adhere to the upper plate, because of down going plate roughness, over-thickened sedimentary cover, or mantle wedge melting (Zhou and Li, 2000; Ducea et al., 2009).The subducting Pacific plate is covered by thick deposits derived from the surrounding orogens, which could inhibit subduction and lead to underplating (Pavlis and Bruhn, 1983). Surveyor submarine fan deposits are up to 4 km thick offshore the Kenai Peninsula and stretch from the St. Elias orogen to the southern edge of Kodiak Island (Reece et al., 2011; Fig. 1). The associated accretionary prism offshore of the Kenai Peninsula has a broad mid-slope terrace unlike the surrounding region along the Aleutian trench, which is indicative of being influenced by a region of a rough down-going plate (Fruehn et al., 1999; von Huene and Klaeschen, 1999). Ye et al. (1997) identified a low velocity zone along the seismic EDGE transect which was interpreted as underplated sediments. In addition, a mid to upper plate discontinuity dipping ~20° to the northwest underneath the Kenai Peninsula was previously discovered by Stephens et al. (1990).Underplating on Kodiak Island is thought to occur near the brittle-ductile transition (~10 km depth) and result in widespread penetrative shortening and exhumation(Clendenen et al., 2003; Carver and Plafker, 2008). Our results imply that the Kenai Mountains are experiencing rock uplift due to forearc growth associated with underplating processes that are comparable to those inferred for the longer history of deformation on Kodiak Island (Pavlis and Bruhn, 1983).

If underplating has been responsible in part for rock uplift of the Kenai Mountains, it is unclear when this process began and what fraction of uplift it is responsible for. Stratigraphic and provenance relationships in Cook Inlet imply that the Kenai Peninsula became emergent in the Late Miocene (Kirschner and Lyon, 1973; Finzel et al., 2011), although it is not clear how high or widespread the mountainous topography was at this time. In contrast, the low exhumation implied by our data suggests that surface uplift has outpaced rock uplift, which we expect should require a recent pulse of surface uplift given the highly erosive nature of the temperate maritime glacial setting. Erosion rates in this setting could easily be >1 km/Ma (Riihimaki et al., 2005; Koppes and Hallet, 2006; Headley et al., 2013), which would have resulted in reset AHe cooling ages and removal of the PRZ in only a few million years. It is thus possible that the Late Miocene emergence of the peninsula involved minimal topographic growth, and that the majority of the Kenai Mountain relief has been produced only in the last few million years. One possible explanation is that the Late Miocene uplift of the Kenai Peninsula resulted from passage of the Yakutat microplate below it. Based on tectonic models, the trailing edge of the microplate should have passed between Kodiak Island and the tip of the Kenai Peninsula at about 3.5 Ma, and subsequently would have tracked north under the Kenai Mountains to its present position (Fig. 1) (DeMets et al., 1990; Von Huene et al., 1998; von Huene and Klaeschen, 1999; Fruehn et al., 1999; Pavlis et al., 2004). Significant underplating may have then begun in the absence of the microplate and arrival of the thickly blanketed subducting slab, resulting in a renewed phase of rock uplift for the Kenai Mountains. If underplating is indeed active beneath the Kenai Mountains, it is possible that continued rock uplift will eventually grow the Kenai Peninsula southwards to eventually connect with Kodiak Island.

6. Conclusions

Although the topography of the Kenai Mountains is rugged, suggesting rapid exhumation, measured AHe ages are older here than in other southern Alaska mountain ranges. These results were only obtainable via extensive replicate dating of sub-optimal apatite grains, given the challenging nature of the local bedrock. The old AHe ages indicate that the Kenai Mountains have not experienced recent, rapid exhumation of sufficient magnitude to reset the AHe thermochronometer (~1–2 km). The Kenai Mountains are therefore distinct from the locus of sustained concentrated rock uplift that has been identified in the Chugach Mountains north of Prince William Sound (Arkle et al., 2013). The minimal exhumation and topographic character suggest that the Kenai Mountains have distinct uplift kinematics from the rest of the coastal orogenic belt to the north and east. We hypothesize that early emergence of the Kenai Peninsula was driven by flat slab subduction, as the trailing edge of the subducting Yakutat plate passed northeastwards below it between the Late Miocene and Pliocene. We further hypothesize that a subsequent, localized pulse of rock uplift has occurred recently in the area of the Kenai Mountains due to underplating associated with thick sediments that sit atop the subducting Pacific Plate. This would make the modern Kenai Mountains analogous to the forearc deformation that has produced Kodiak Island. These findings illustrate the dynamic, localized complexity of emergent forearc deformation in response to the variation in orientation and character of subducting slabs. The results also suggest that the Kenai Mountains are an unusual orogen that is in disequilibrium with the local erosional setting, presumably due to recent onset or acceleration of surface uplift. Despite the potential for aggressive glacial erosion given the local climate, erosion significantly lags behind rock uplift.

Acknowledgments

We thank Jeanette Arkle and Michelle Fame for helpful discussions and Jon Smith for assistance with lab work and sample preparation. We want to thank Peter Haeussler and Terry Pavlis for their helpful and thorough reviews of this manuscript. Support was provided by the National Science Foundation grant EAR-1123688/1123643.

References

Abers, G.A., 2008. Orogenesis from subducting thick crust and evidence from Alaska. Active Tectonics and Seismic Potential of Alaska vol. 179. American Geophysical Union Monograph Series, pp. 337–349.

Arkle, J., Armstrong, P., Haeussler, P., Prior, M., Hartman, S., Sendziak, K., Brush, J., 2013. Focused exhumation in the syntaxis of the western Chugach Mountains and Prince

William Sound, Alaska. Geol. Soc. Am. Bull. 125 (5–6), 776–793. http://dx.doi.org/10.1130/b30738.1.
Berger, A.L., Spotila, J.A., Chapman, J.B., Pavlis, T.L., Enkelmann, E., Ruppert, N.A., Buscher, J.T., 2008. Architecture, kinematics, and exhumation of a convergent orogenic wedge: a thermochronological investigation of tectonic–climatic interactions within the central St. Elias Orogen, Alaska. Earth Planet. Sci. Lett. 270 (1–2), 13–24. http://dx.doi.org/10.1016/j.epsl.2008.02.034.
Bol, A.J., Roeske, S., 1993. Strike–slip faulting and block rotation along the Contact fault system, Prince William sound Alaska. Tectonics 12 (1), 49–62.
Bradley, D.C., Parrish, R., Clendenen, W., Lux, D., Layer, P., Heizler, M., Donley, D.T., 2000. New geochronological evidence for the timing of early Tertiary ridge subduction in southern Alaska. US Geol. Surv. Prof. Pap. 1615, 5–21.
Brandon, M.T., Roden-Tice, M.K., Garver, J.I., 1998. Late Cenozoic exhumation of the Cascadia accretionary wedge in the Olympic Mountains, northwest Washington State. Geol. Soc. Am. Bull. 110 (8), 985–1009.
Brown, R.W., Beucher, R., Roper, S., Persano, C., Stuart, F., Fitzgerald, P., 2013. Natural age dispersion arising from the analysis of broken crystals. Part I: theoretical basis and implications for the apatite (U–Th)/He thermochronometer. Geochim. Cosmochim. Acta 122 (0), 478–497. http://dx.doi.org/10.1016/j.gca.2013.05.041.
Bruhn, R., Haeussler, P., 2006. Deformation driven by subduction and microplate collision: geodynamics of Cook Inlet basin, Alaska. Geol. Soc. Am. Bull. 118 (3–4), 289–303. http://dx.doi.org/10.1130/b25672.1.
Bruhn, R., Pavlis, T., Plafker, G., Serpa, L., 2004. Deformation during terrane accretion in the Saint Elias orogen, Alaska. Geol. Soc. Am. Bull. 116 (7–8), 771–787. http://dx.doi.org/10.1130/b25182.1.
Buscher, J.T., Berger, A.L., Spotila, J.A., 2008. Exhumation in the Chugach–Kenai Mountain Belt above the Aleutian Subduction Zone, Southern Alaska. Active Tectonics and Seismic Potential of Alaska vol. 179. American Geophysical Union Monograph Series, pp. 151–166.
Carver, G., Plafker, G., 2008. Paleoseismicity and neotectonics of the Aleutian subduction zone—An overview. Active Tectonics and Seismic Potential of Alaska, pp. 43–63.
Christeson, G., Gulick, S., van Avendonk, H., Worthington, L., Reece, R., Pavlis, T., 2010. The Yakutat terrane: dramatic change in crustal thickness across the Transition fault, Alaska. Geology 38 (10), 895–898. http://dx.doi.org/10.1130/g31170.1.
Clendenen, W.S., Fisher, D., Byrne, T., 2003. Cooling and Exhumation History of the Kodiak Accretionary Prism, Southwest Alaska. Special Papers, Geological Society of America, pp. 71–88.
Cohen, S.C., Freymueller, J.T., 1997. Deformation of the Kenai Peninsula, Alaska. J. Geophys. Res. 102 (B9), 20479–20487. http://dx.doi.org/10.1029/97JB01513.
DeMets, C., Gordon, R.G., Argus, D.F., Stein, S., 1990. Current plate motions. Geophys. J. Int. 101, 425–478.
Dominguez, S., Malavieille, J., Lallemand, S.E., 2000. Deformation of accretionary wedges in response to seamount subduction: insights from sandbox experiments. Tectonics 19 (1), 182–196.
Ducea, M., Kidder, S., Chesley, J., Saleeby, J., 2009. Tectonic underplating of trench sediments beneath magmatic arcs: the central California example. Int. Geol. Rev. 51 (1), 1–26. http://dx.doi.org/10.1080/00206810802602767.
Dumitru, T.A., Gans, P.B., Foster, D.A., Miller, E.L., 1991. Refrigeration of the western Cordilleran lithosphere during Laramide shallow-angle subduction. Geology 19 (11), 1145–1148.
Eberhart-Phillips, D., Christensen, D.H., Brocher, T.M., Hansen, R., Ruppert, N.A., Haeussler, P.J., Abers, G.A., 2006. Imaging the transition from Aleutian subduction to Yakutat collision in central Alaska, with local earthquakes and active source data. J. Geophys. Res. Solid Earth 111 (B11). http://dx.doi.org/10.1029/2005JB004240.
Ehlers, T.A., Farley, K.A., 2003. Apatite (U–Th)/He thermochronometry: methods and applications to problems in tectonic and surface processes. Earth Planet. Sci. Lett. 206 (1–2), 1–14. http://dx.doi.org/10.1016/S0012-821X(02)01069-5.
Elliott, J.L., Larsen, C.F., Freymueller, J.T., Motyka, R.J., 2010. Tectonic block motion and glacial isostatic adjustment in southeast Alaska and adjacent Canada constrained by GPS measurements. J. Geophys. Res. 115, B09407. http://dx.doi.org/10.1029/2009JB007139.
English, J.M., Johnston, S.T., Wang, K., 2003. Thermal modelling of the Laramide orogeny: testing the flat-slab subduction hypothesis. Earth Planet. Sci. Lett. 214 (3–4), 619–632. http://dx.doi.org/10.1016/S0012-821X(03)00399-6.
Enkelmann, E., Zeitler, P.K., Garver, J.I., Pavlis, T.L., Hooks, B.P., 2010. The thermochronological record of tectonic and surface process interaction at the Yakutat–North American collision zone in Southeast Alaska. Am. J. Sci. 310 (4), 231–260.
Enkelmann, E., Koons, P.O., Pavlis, T.L., Hallet, B., Barker, A., Elliott, J., Garver, J.I., Gulick, S.P.S., Headley, R.M., Pavlis, G.L., et al., 2015. Cooperation among tectonic and surface processes in the St. Elias Range, Earth's highest coastal mountains. Geophys. Res. Lett. 42, 5838–5846. http://dx.doi.org/10.1002/2015GL064727.
Farley, K.A., 2000. Helium diffusion from apatite: General behavior as illustrated by Durango fluorapatite. J. Geophys. Res. 105 (B2), 2903–2914. http://dx.doi.org/10.1029/1999JB900348.
Ferguson, K., Armstrong, P., Arkle, J., Haeussler, P., 2015. Focused rock uplift above the subduction décollement at Montague and Hinchinbrook Islands, Prince William Sound, Alaska. Geosphere 11 (1), 144–159. http://dx.doi.org/10.1130/ges01036.1.
Ferris, A., Abers, G.A., Christensen, D.H., Veenstra, E., 2003. High resolution image of the subducted Pacific (?) plate beneath central Alaska, 50–150 km depth. Earth Planet. Sci. Lett. 214 (3–4), 575–588. http://dx.doi.org/10.1016/S0012-821X(03)00403-5.
Finzel, E.S., Trop, J.M., Ridgway, K.D., Enkelmann, E., 2011. Upper plate proxies for flat-slab subduction processes in southern Alaska. Earth Planet. Sci. Lett. 303 (3–4), 348–360. http://dx.doi.org/10.1016/j.epsl.2011.01.014.
Fisher, M.A., Magoon, L.B., 1978. Geologic framework of lower Cook inlet, Alaska. AAPG Bull. 62 (3), 373–402.
Fisher, D.M., Gardner, T.W., Marshall, J.S., Sak, P.B., Protti, M., 1998. Effect of subducting sea-floor roughness on fore-arc kinematics, Pacific coast, Costa Rica. Geology 26 (5), 467–470.
Fletcher, H.J., Freymueller, J.T., 1999. New GPS constraints on the motion of the Yakutat block. Geophys. Res. Lett. 26 (19), 3029–3032.
Flowers, R.M., Ketcham, R.A., Shuster, D.L., Farley, K.A., 2009. Apatite (U–Th)/He thermochronometry using a radiation damage accumulation and annealing model. Geochim. Cosmochim. Acta 73 (8), 2347–2365. http://dx.doi.org/10.1016/j.gca.2009.01.015.
Freeland, G.L., Dietz, R.S., 1973. Rotation history of Alaskan tectonic blocks. Tectonophysics 18 (3–4), 379–389. http://dx.doi.org/10.1016/0040-1951(73)90054-1.
Freymueller, J.T., Woodard, H., Cohen, S.C., Cross, R., Elliott, J., Larsen, C.F., Hreinsdóttir, S., Zweck, C., 2008. Active deformation processes in Alaska, based on 15 years of GPS measurements. Active Tectonics and Seismic Potential of Alaska, (pp. 1–42). American Geophysical Union Geophysics Monograph Series 179.
Fruehn, J., von Huene, R., Fisher, M.A., 1999. Accretion in the wake of terrane collision: the Neogene accretionary wedge off Kenai Peninsula, Alaska. Tectonics 18 (2), 263–277. http://dx.doi.org/10.1029/1998TC900021.
Fuis, G., Moore, T., Plafker, G., Brocher, T., Fisher, M., Mooney, W., Nokleberg, W., Page, R., Beaudoin, B., Christensen, N., Levander, A., Lutter, W., Saltus, R., Ruppert, N., 2008. Trans-Alaska Crustal Transect and continental evolution involving subduction underplating and synchronous foreland thrusting. Geology 36 (3), 267–270. http://dx.doi.org/10.1130/g24257a.1.
Gardner, T., Fisher, D., Morell, K., Cupper, M., 2013. Upper-plate deformation in response to flat slab subduction inboard of the aseismic Cocos Ridge, Osa Peninsula, Costa Rica. Lithosphere 5 (3), 247–264. http://dx.doi.org/10.1130/l251.1.
Gutscher, M.A., Maury, R., Eissen, J.P., Bourdon, E., 2000. Can slab melting be caused by flat subduction? Geology 28 (6), 535–538. http://dx.doi.org/10.1130/0091-7613(2000)28<535:csmbcb>2.0.co;2.
Haeussler, P.J., 2008. An overview of the Neotectonics of interior Alaska: far-field deformation from the Yakutat microplate collision. Active Tectonics and Seismic Potential of Alaska. American Geophysical Union Geophysics Monograph Series 179, pp. 83–108.
Haeussler, P.J., Saltus, R.W., 2011. Location and Extent of Tertiary Structures in Cook Inlet Basin, Alaska, and Mantle Dynamics that Focus Deformation and Subsidence (No. 1776-D, pp. i-26). US Geological Survey.
Haeussler, P., Bruhn, R., Pratt, T., 2000. Potential seismic hazards and tectonics of the upper Cook Inlet basin, Alaska, based on analysis of Pliocene and younger deformation. Geol. Soc. Am. Bull. 112 (9), 1414–1429. http://dx.doi.org/10.1130/0016-7606(2000)112<1414:pshato>2.0.co;2.
Haeussler, P., Bradley, D., Wells, R., Miller, M., 2003. Life and death of the Resurrection plate: evidence for its existence and subduction in the northeastern Pacific in Paleocene–Eocene time. Geol. Soc. Am. Bull. 115 (7), 867–880. http://dx.doi.org/10.1130/0016-7606(2003)115<0867:ladotr>2.0.co;2.
Haeussler, P.J., Armstrong, P.A., Liberty, L.M., Ferguson, K.M., Finn, S.P., Arkle, J.C., Pratt, T.L., 2015. Focused exhumation along megathrust splay faults in Prince William Sound, Alaska. Quat. Sci. Rev. 113, 8–22.
Hartman, D.C., Pessel, G.H., McGee, D.L., 1974. Stratigraphy of the Kenai Group, Cook Inlet. Alaska Division of Geological and Geophysical Surveys. Alaska Open File Report 49.
Headley, R.M., Enkelmann, E., Hallet, B., 2013. Examination of the interplay between glacial processes and exhumation in the Saint Elias Mountains, Alaska. Geosphere 9 (2), 229–241.
Helwig, J., Emmet, P., 1981. Structure of the Early Tertiary Orca Group in Prince William Sound and some implications for the plate tectonic history of southern Alaska. J. Alaska Geol. Soc. 1, 12–35.
Karlstrom, T.N.V., 1961. The glacial history of Alaska: it's bearing on paleoclimatic history. Ann. N. Y. Acad. Sci. 95 (1), 290–340. http://dx.doi.org/10.1111/j.1749-6632.1961.tb50040.x.
Kirschner, C.E., Lyon, C.A., 1973. Stratigraphic and Tectonic Development of Cook Inlet Petroleum Province. Regional Arctic Geology of Alaska, pp. 396–407.
Koppes, M., Hallet, B., 2006. Erosion rates during rapid deglaciation in Icy Bay, Alaska. J. Geophys. Res. Earth Surf. 111 (F2).
Li, Z.X., Li, X.H., 2007. Formation of the 1300-km-wide intracontinentalorogen and postorogenic magmatic province in Mesozoic South China: a flat-slab subduction model. Geology 35 (2), 179–182. http://dx.doi.org/10.1130/g23193a.1.
Little, T.A., Naeser, C.W., 1989. Tertiary tectonics of the Border Ranges Fault System, Chugach Mountains, Alaska: deformation and uplift in a forearc setting. J. Geophys. Res. 94 (B4), 4333–4359. http://dx.doi.org/10.1029/JB094iB04p0433.
Magoon, L.B., 1986. Present-day geothermal gradient. U.S. Geol. Surv. Bull. (B-1596), 41–46.
Mankhemthong, N., Doser, D.I., Pavlis, T.L., 2013. Interpretation of gravity and magnetic data and development of two-dimensional cross-sectional models for the Border Ranges fault system, south-central Alaska. Geosphere 9 (2), 242–259.
Mann, D.H., Peteet, D.M., 1994. Extent and timing of the Last Glacial Maximum in Southwestern Alaska. Quat. Res. 42 (2), 136–148. http://dx.doi.org/10.1006/qres.1994.1063.
Mazzotti, S., Hyndman, R., 2002. Yakutat collision and strain transfer across the northern Canadian Cordillera. Geology 30 (6), 495–498. http://dx.doi.org/10.1130/0091-7613(2002)030<0495:ycasta>2.0.co;2.
National Climate Data Center, 2005. Kenai municipal airport weather station data. [online]. Available from http://www.ncdc.noaa.gov/cdo-web/quickdata ([cited 16December 2015]).
National Climate Data Center, 2007. Seward meteorological station. [online]. Available from http://www.ncdc.noaa.gov/cdo-web/quickdata ([cited 16 December 2015]).
Oskin, M., Burbank, D.W., 2005. Alpine landscape evolution dominated by cirque retreat. Geology 33 (12), 933–936.

Ouimet, W.B., Whipple, K.X., Granger, D.E., 2009. Beyond threshold hillslopes: channel adjustment to base-level fall in tectonically active mountain ranges. Geology 37 (7), 579–582.

Parry, W.T., Bunds, M.P., Bruhn, R.L., Hall, C.M., Murphy, J.M., 2001. Mineralogy, $^{40}Ar/^{39}Ar$ dating and apatite fission track dating of rocks along the Castle Mountain fault, Alaska. Tectonophysics 337 (3–4), 149–172. http://dx.doi.org/10.1016/S0040-1951(01)00117-2.

Pavlis, T.L., Bruhn, R.L., 1983. Deep-seated flow as a mechanism for the uplift of broad forearc ridges and its role in the exposure of high P/T metamorphicterranes. Tectonics 2 (5), 473–497. http://dx.doi.org/10.1029/TC002i005p00473.

Pavlis, T.L., Roeske, S.M., 2007. The Border Ranges fault system, southern Alaska. Geol. Soc. Am. Spec. Pap. 431, 95–127.

Pavlis, T.L., Picornell, C., Serpa, L., Bruhn, R.L., Plafker, G., 2004. Tectonic processes during oblique collision: insights from the St. Elias orogen, northern North American Cordillera. Tectonics 23 (3).

Peacock, S.M., 1996. Thermal and petrologic structure of subduction zones. Subduction: Top to Bottom. AGU Geophysical Monograph 96, Washington, D.C., pp. 119–133.

Perry, S.E., Garver, J.I., Ridgway, K.D., 2009. Transport of the Yakutat Terrane, Southern Alaska: evidence from sediment petrology and detrital zircon fission-track and U/Pb double dating. J. Geol. 117 (2), 156–173. http://dx.doi.org/10.1086/596302.

Péwé, T.L., 1975. Quaternary Geology of Alaska. U.S. Geological Survey Professional Paper 835, p. 145.

Plafker, G., 1969. Tectonics of the March 27, 1964, Alaska Earthquake. US Government Printing Office, p. 74.

Plafker, G., 1987. Regional geology and petroleum potential of the northern Gulf of Alaska continental margin. In: Scholl, D.W., Grantz, A., Vedder, J.G. (Eds.), Geology and Resource Potential of the Continental Margin of Western North America and Adjacent Ocean Basins—Beaufort Sea to Baja California: Circum-Pacific Council for Energy and Mineral Resources. Earth Sciences Series, 6, 299–268.

Plafker, G., Berg, H.C., 1994. Overview of the geology and tectonic evolution of Alaska. In: Plafker, G., Berg, H.C. (Eds.), The Geology of Alaska vol. G-1. Geological Society of America, Geology of North America, Boulder, Colorado, pp. 989–1021.

Plafker, G., Nokleberg, W.J., Lull, J.S., 1989. Bedrock geology and tectonic evolution of the Wrangellia, Peninsular, and Chugach Terranes along the Trans-Alaska Crustal Transect in the Chugach Mountains and Southern Copper River Basin, Alaska. J. Geophys. Res. 94 (B4), 4255–4295. http://dx.doi.org/10.1029/JB094iB04p04255.

Plattner, C., Malservisi, R., Dixon, T.H., LaFemina, P., Sella, G.F., Fletcher, J., Suarez-Vidal, F., 2007. New constraints on relative motion between the Pacific Plate and Baja California microplate (Mexico) from GPS measurements. Geophys. J. Int. 170 (3), 1373–1380. http://dx.doi.org/10.1111/j.1365-246x.2007.03494.x.

Ramos, V.A., Cristallini, E.O., Pérez, D.J., 2002. The Pampean flat-slab of the Central Andes. J. S. Am. Earth Sci. 15 (1), 59–78. http://dx.doi.org/10.1016/S0895-9811(02)00006-8.

Reece, R.S., Gulick, S.P., Horton, B.K., Christeson, G.L., Worthington, L.L., 2011. Tectonic and climatic influence on the evolution of the Surveyor Fan and Channel system, Gulf of Alaska. Geosphere 7 (4), 830–844.

Riccio, S.J., Fitzgerald, P.G., Benowitz, J.A., Roeske, S.M., 2014. The role of thrust faulting in the formation of the eastern Alaska Range: thermochronological constraints from the Susitna Glacier Thrust Fault region of the intracontinental strike–slip Denali Fault system. Tectonics 33, 2195–2217. http://dx.doi.org/10.1002/2014TC003646.

Ridgway, K., Thoms, E., Layer, P., Lesh, M., White, J., Smith, S., 2007. Neogene transpressional foreland basin development on the north side of the central Alaska Range, Usibelli Group and Nenana Gravel, Tanana basin. Geol. Soc. Am. Spec. Pap. 431, 507–547. http://dx.doi.org/10.1130/2007.2431(20).

Ridgway, K.D., Trop, J.M., Finzel, E.S., 2011. Modification of continental forearc basins by flat-slab subduction processes: a case study from Southern Alaska. Tectonics of Sedimentary Basins. John Wiley & Sons, Ltd, pp. 327–346.

Riihimaki, C.A., MacGregor, K.R., Anderson, R.S., Anderson, S.P., Loso, M.G., 2005. Sediment evacuation and glacial erosion rates at a small alpine glacier. J. Geophys. Res. Earth Surf. 110 (F3).

Spotila, J.A., Berger, A.L., 2010. Exhumation at orogenic indentor corners under long-term glacial conditions: example of the St. Elias orogen, Southern Alaska. Tectonophysics 490 (3–4), 241–256. http://dx.doi.org/10.1016/j.tecto.2010.05.015.

Spotila, J.A., Buscher, J.T., Meigs, A.J., Reiners, P.W., 2004. Long-term glacial erosion of active mountain belts: example of the Chugach–St. Elias Range, Alaska. Geology 32 (6), 501–504.

Stephens, C.D., Page, R.A., Lahr, J.C., 1990. Reflected and mode-converted seismic waves within the shallow Aleutian Subduction Zone, Southern Kenai Peninsula, Alaska. J. Geophys. Res. Solid Earth 95 (B5), 6883–6897. http://dx.doi.org/10.1029/JB095iB05p06883.

von Huene, R.V., Klaeschen, D., 1999. Opposing gradients of permanent strain in the aseismic zone and elastic strain across the seismogenic zone of the Kodiak shelf and slope, Alaska. Tectonics 18 (2), 248–262.

Von Huene, R., Klaeschen, D., Gutscher, M., Fruehn, J., 1998. Mass and fluid flux during accretion at the Alaskan margin. Geol. Soc. Am. Bull. 110 (4), 468–482.

Westaway, R., 2006. Cenozoic cooling histories in the Menderes Massif, western Turkey, may be caused by erosion and flat subduction, not low-angle normal faulting. Tectonophysics 412 (1), 1–25.

Wiles, G.C., Calkin, P.E., Post, A., 1995. Glacier fluctuations in the Kenai Fjords, Alaska, U.S.A.: an evaluation of controls on iceberg-calving glaciers. Arct. Alp. Res. 27 (3), 234–245. http://dx.doi.org/10.2307/1551954.

Willis, J.B., Haeussler, P.J., Bruhn, R.L., Willis, G.C., 2007. Holocene slip rate for the western segment of the Castle Mountain fault, Alaska. Bull. Seismol. Soc. Am. 97 (3), 1019–1024.

Worthington, L.L., Van Avendonk, H.J.A., Gulick, S.P.S., Christeson, G.L., Pavlis, T.L., 2012. Crustal structure of the Yakutat terrane and the evolution of subduction and collision in southern Alaska. J. Geophys. Res. 117, B01102. http://dx.doi.org/10.1029/2011JB008493.

Ye, S., Flueh, E.R., Kaeschen, D., Von Huene, R., 1997. Crustal structure along the EDGE transect beneath the Kodiak Shelf off Alaska derived from OBH seismic refraction data. Geophys. J. Int. 130, 283–302. http://dx.doi.org/10.1111/j.1365-246X.1997.tb05648.x.

Zhou, X.M., Li, W.X., 2000. Origin of Late Mesozoic igneous rocks in Southeastern China: implications for lithosphere subduction and underplating of mafic magmas. Tectonophysics 326 (3), 269–287.